Available online at www.sciencedirect.com
SCIENCE DIRECT®
Journal of Computational Physics 200 (2004) 325–346
JOURNAL OF COMPUTATIONAL PHYSICS
www.elsevier.com/locate/jcp

A class of fully second order accurate projection methods for solving the incompressible Navier–Stokes equations

Miao'er Liu [a], Yu-Xin Ren [a,*], Hanxin Zhang [b]

[a] *Department of Engineering Mechanics, Tsinghua University, Beijing 100084, China*
[b] *National Key Laboratory for CFD, Beijing 100083, China*

Received 30 October 2003; received in revised form 27 February 2004; accepted 13 April 2004
Available online 28 May 2004

Abstract

In this paper, a continuous projection method is designed and analyzed. The continuous projection method consists of a set of partial differential equations which can be regarded as an approximation of the Navier–Stokes (N–S) equations in each time interval of a given time discretization. The local truncation error (LTE) analysis is applied to the continuous projection methods, which yields a sufficient condition for the continuous projection methods to be temporally second order accurate. Based on this sufficient condition, a fully second order accurate discrete projection method is proposed. A heuristic stability analysis is performed to this projection method showing that the present projection method can be stable. The stability of the present scheme is further verified through numerical experiments. The second order accuracy of the present projection method is confirmed by several numerical test cases.

AMS: 65M06; 76D05; 65M15

Keywords: Incompressible Navier–Stokes equations; Projection methods; Artificial boundary conditions; Local truncation error

1. Introduction

The difficulty in numerically solving the unsteady incompressible Navier–Stokes (N–S) equations in primitive variable form arises from the specific velocity–pressure coupling. In the 1960s, Chorin observed that for incompressible flows, the pressure did not carry any thermodynamic meaning and was presented only as a Lagrange multiplier to enforce the incompressibility constraint. This observation motivated an operator-splitting discretization scheme known as the projection method or the fractional step method [5,6], in which the computations of the velocity and the pressure are decoupled through a two-step predictor–corrector procedure. In the first step, an intermediate velocity field is computed by solving the momentum

* Corresponding author. Tel.: +86-10-62785543; fax: +86-10-62781824.
E-mail address: ryx@tsinghua.edu.cn (Y.-X. Ren).

0021-9991/$ - see front matter
doi:10.1016/j.jcp.2004.04.006

equations ignoring the pressure term and the incompressibility constraint; in the second step, according to Helmholtz–Hodge decomposition theorem [11], the intermediate velocity is projected to the space of the divergence-free vector fields to get the pressure and the corrected velocity that satisfies the incompressibility condition. Because of the decoupling of the velocity and the pressure computations, the projection method is much more efficient than the fully coupled procedures. This notable advantage has attracted great attention, and many improved projection methods have been seen in publications [1–4,21,22,33] of the past 20 years. The projection methods are currently among the most popular methods for solving viscous incompressible flow based on the primitive variable formulations.

Despite the advantages, the velocity–pressure decoupling adversely affects the temporal accuracy of the numerical scheme. In previous works [4,9,10,17,29–32,36], many efforts have been devoted to the improvement of the temporal accuracy of the projection methods. It has been observed both numerically and analytically that while a temporally second order convergence for the velocity can be readily obtained, the computed pressure is typically only first order accurate in time [6]. Some authors have attributed the first order temporal accuracy to the inappropriate boundary conditions for the intermediate variables [4,13,17,20–22,25,28], and others speculated that the projection methods are inherently first order in time for the pressure and cannot be improved to a higher order accuracy [26].

It should be noted that in the construction of the projection or the fractional step schemes, two methods with subtle differences are often used. The relative new but more straightforward method was due to Dukowicz and Dvinsky [7], who proposed to construct the fractional step method through the approximate block LU factorization of the fully discrete incompressible N–S equations written in block matrix form. This method has been further developed by Perot [26] and others [19,27]. Because of the factorization nature of this approach, the "artificial" boundary conditions for the intermediate velocity are not required. Another method, following the original work of Chorin, was to present the projection methods in semi-discrete formulations with the temporal derivatives being discretized and the spatial derivatives remaining in their continuous forms. When these semi-discrete formulations are numerically solved after spatial discretizations, certain "artificial" boundary conditions for the intermediate velocity must be used. These two approaches are in close relations: the first approach can be used to derive the artificial boundary conditions needed by the second approach; and the second approach, with different artificial boundary conditions, can be also regarded as the first method using different approximate block LU factorizations. Because the second approach is in closer relation to the work that will be presented in the present paper, and also because the second approach is independent of any particular spatial discrete scheme, the projection or fractional step methods based on the second approach will be reviewed in a little bit more detail in the following several passages.

In order to construct higher order projection methods using the second approach, two ingredients should be regarded: the pressure updating formulation and the artificial boundary conditions. Brown et al. [4] have pointed out the importance of the pressure updating formulation. By performing the normal mode analysis, they showed that when a consistent pressure updating formulation was used together with proper boundary conditions, second order temporal accuracy was able to achieved for both velocity and pressure fields. (In a general domain, however, 3/2-order accuracy for the pressure appeared to be best possible based on the results of [17].) When the pressure updating formulation was not consistent with N–S equations, the velocity could still be second order accurate in time, but some pseudo-modes appeared in the pressure field, which would produce the pressure numerical boundary layer and the resulted pressure field was only first order in time.

It is well known that the intermediate velocity has not any physical meaning, and requires artificial boundary conditions. Kim and Moin [22] noticed that the tangential velocity will loss its accuracy near boundary and produce a numerical boundary layer in their pressure-free projection method when the boundary conditions used for the intermediate velocity is the same as that for the physical velocity. As a remedy, a Taylor series expansion technique was used to obtain higher order approximation in tangential

component of the intermediate velocity on the boundary. After modifying the artificial boundary conditions, second order accuracy for the velocity was obtained, although the first order accuracy for the pressure remained [4].

Recently, Iannelli and Denaro [20] have analyzed the pressure-free projection method in terms of its local truncation error (LTE). They concluded that the pressure-free projection method both in continuous and discrete sense could be inherently second order accurate for the velocity when appropriate boundary conditions was used, regardless of the pressure accuracy. They also recommended new artificial boundary conditions by which the velocity could be second order accurate up to the boundaries.

Motivated by these previous works, the temporal accuracy of the projection method is discussed in terms of LTE analysis technique in the present paper. In the present paper, the analysis is based on the so-called continuous projection scheme which consists of a set of partial differential equations approximating the original N–S (or corresponding Stokes) equations to a certain order. This set of equations is designed so that when it is discretized, the resulting equations are nothing but the standard projection schemes in discrete forms. The advantage of the continuous projection method is that we can analyze the accuracy of this method independent of both temporal and spatial discretization procedures. The sound mathematical behavior of the continuous differential operators also makes it relatively easy to analysis the properties of the continuous projection method.

The LTE analysis of a general class of continuous projection methods for both the velocity and pressure fields is carried out in the present paper. We find that the rigorous LTE analysis is possible only under artificial boundary conditions in specific forms. These specific forms of the artificial boundary conditions can be used in turn to design higher order projection methods. As a result of this LTE analysis, a class of fully second order accurate projection methods is developed. The second order accuracy for both the velocity and the pressure fields is verified through numerical tests. A heuristic stability analysis is performed, which shows that the present projection method can be stable. The stability of the present scheme is further verified through numerical experiments.

This paper is organized as follows. In Section 2, the continuous projection method is identified and presented. In Section 3, the LTE analysis of the continuous projection methods is discussed and the appropriate boundary conditions of the intermediate velocity for the fully second order projection methods are derived. Section 4 presents the numerical discretization of the continuous projection method. A heuristic stability analysis of the discrete projection method is also provided in this section. Section 5 displays the numerical results and the conclusions are given in Section 6.

2. The continuous projection methods

The unsteady incompressible N–S equations in primitive variable form can be written as

$$\frac{\partial \boldsymbol{u}}{\partial t} + \nabla p = -(\boldsymbol{u}\cdot\nabla)\boldsymbol{u} + \upsilon\nabla^2\boldsymbol{u} + \boldsymbol{f}, \tag{1}$$

$$\nabla\cdot\boldsymbol{u} = 0,$$

where $\boldsymbol{u}$, p, υ, $\boldsymbol{f}$ are the velocity vector, pressure, kinematic viscosity of the fluid, and body force, respectively. The density is already absorbed in the pressure term and is not shown in Eq. (1). The initial conditions are

$$\boldsymbol{u}(\boldsymbol{x}, 0) = \boldsymbol{u}_0,$$

and the boundary conditions are

$$\boldsymbol{u}_b = \boldsymbol{w}.$$

In the projection or the fractional step methods, the convection terms are usually discretized explicitly by, for example, the Adams–Bashforth scheme [4,9,10,20–22,33]. For simplicity, we omit the convection terms and consider only the Stokes equations in the present and the following two sections. However, in the numerical experiments presented in Section 5, the N–S equations are actually solved. It should be noted that it is a common practice to analyze the temporal accuracy of the projection methods in terms of the Stokes equations [4]. The results of the LTE analysis can be extended to the N–S equations readily. The Stokes equations are written in the following form:

$$\frac{\partial \boldsymbol{u}}{\partial t} = \upsilon \Delta \boldsymbol{u} - \nabla p + \boldsymbol{f}, \tag{2}$$

$$\nabla \cdot \boldsymbol{u} = 0, \tag{3}$$

with the same initial and boundary conditions as the N–S equations.

In this section, the continuous projection method will be identified and presented. In this approach, giving a discretization in time denoted by $t^j = j\Delta t$ $(j = 0, 1, \ldots)$, we will introduce some intermediate variables and construct a set of partial differential equations which approximates the N–S equations (or the Stokes equations in this section) to certain order of accuracy within every time interval $[t^n, t^{n+1}]$. Because of the introduction of new variables, the artificial boundary conditions for these variables are needed. The advantage of this approach is that we can analyze the accuracy of these equations independent of any spatial and temporal discretization procedures. That is to say, if these equations are the kth order approximation of the original N–S (or Stokes) equations, then any kth or higher order discretization of them will approximate the N–S (or Stokes) equations to kth order. The sound mathematical behavior of the continuous differential operators makes it relatively easy to analysis the properties of these equations. In this paper, these partial differential equations are designed so that when they are discretized, the resulting algebraic equations are nothing but the standard projection schemes in discrete forms. Therefore, this approach is called the continuous projection method in the present paper. We should note that the temporal discretizations of these equations will always be performed between t^n and t^{n+1}. We assume that the flow variables are known when $t \leqslant t^n$, and the discrete projection method is used to evaluate the flow variables at time t^{n+1}.

At each time interval, such as that between t^n and t^{n+1}, we introduce two intermediate variables $\boldsymbol{u}^*$ and q, and require

$$\frac{\partial \boldsymbol{u}^*}{\partial t} = \upsilon \Delta \boldsymbol{u}^* - \nabla q + \boldsymbol{f}, \tag{4}$$

where $\boldsymbol{u}^*$ is the intermediate velocity vector and q is an approximation of the pressure p . The initial and boundary conditions of Eq. (4) are, respectively,

$$(\boldsymbol{u}^*)^n = \tilde{\boldsymbol{u}}^n \tag{5}$$

and

$$\boldsymbol{u}^*_{\mathrm{b}} = \boldsymbol{w} + \nabla \psi, \tag{6}$$

where $\tilde{\boldsymbol{u}}^n$ is the approximate solution of the velocity at the previous time step, and ψ is an expression in the boundary conditions with its form to be determined.

Once we have obtained the $\boldsymbol{u}^*$ by means of Eqs. (4)–(6), according to the Helmholtz–Hodge theorem [11], $\boldsymbol{u}^*$ can be decomposed into

$$\boldsymbol{u}^* = \tilde{\boldsymbol{u}} + \nabla\phi, \tag{7}$$

in which $\tilde{\boldsymbol{u}}$ is the solution of the continuous projection method and satisfies

$$\nabla \cdot \tilde{\boldsymbol{u}} = 0. \tag{8}$$

Eqs. (7) and (8) give a Poisson equation

$$\nabla^2\phi = \nabla \cdot \boldsymbol{u}^*. \tag{9}$$

To get the boundary condition of Eq. (9), we consider Eq. (7) on the boundaries

$$\boldsymbol{u}^*_{\mathrm{b}} = \tilde{\boldsymbol{u}}_{\mathrm{b}} + \nabla\phi_{\mathrm{b}}.$$

It is easy to derive that

$$\nabla\phi_{\mathrm{b}} = \nabla\psi - (\tilde{\boldsymbol{u}}_{\mathrm{b}} - \boldsymbol{w}). \tag{10}$$

Usually, the normal component of Eq. (10) is chosen as the boundary conditions of Eq. (9) [15,21]. If we require additionally that

$$\boldsymbol{w} \cdot \boldsymbol{n} = \tilde{\boldsymbol{u}}_{\mathrm{b}} \cdot \boldsymbol{n},$$

where $\boldsymbol{n}$ is a unit vector normal to the boundaries, the boundary condition for Eq. (9) can be written as

$$\frac{\partial\phi_{\mathrm{b}}}{\partial n} = \frac{\partial\psi}{\partial n}. \tag{11}$$

By solving Eq. (9) with the boundary condition (11), one can get ϕ, and $\tilde{\boldsymbol{u}}$ can be obtained accordingly from Eq. (7).

Plugging Eq. (7) into Eq. (4), the following equation is obtained

$$\frac{\partial\tilde{\boldsymbol{u}}}{\partial t} = \upsilon\Delta\tilde{\boldsymbol{u}} - \nabla\left[q + \frac{\partial\phi}{\partial t} - \upsilon\Delta\phi\right] + \boldsymbol{f}. \tag{12}$$

We require that Eq. (12) is consistent with Eq. (2) for arbitrary t ($t^n \leqslant t \leqslant t^{n+1}$), or more specifically, we regard $\tilde{\boldsymbol{u}}$ and $\tilde{p}$ as the solutions of

$$\frac{\partial\tilde{\boldsymbol{u}}}{\partial t} = \upsilon\Delta\tilde{\boldsymbol{u}} - \nabla\tilde{p} + \boldsymbol{f}, \tag{13}$$

and Eq. (8). Comparing Eq. (12) with Eq. (13), it is clear that $\tilde{p}$ has to be computed by

$$\tilde{p} = q + \frac{\partial\phi}{\partial t} - \upsilon\Delta\phi. \tag{14}$$

Eq. (14) [34] is called the consistent pressure updating equation. The importance of the consistency in the pressure updating equation in discrete form has been discussed in [4,16,17].

Eqs. (4), (7), (9) and (14) constitute the governing equations of the continuous projection method. In Section 3, we will show that with proper artificial boundary conditions, this set of equations is a second order approximation of the original Stokes equations.

Remark. The continuous projection method is in close relation with the gauge method [8,24,35]. In fact, if $\boldsymbol{u}^*$ and ϕ are taken as the auxiliary field and the gauge variable (denoted by $\boldsymbol{a}$ and φ), respectively, the governing equations of the continuous projection method are quite similar to those of the gauge method. However, there are some differences between these two methods.

The first and the most important difference is that the equations of the continuous projection method are defined locally within a time step. Therefore, the $\boldsymbol{u}^*$ and ϕ, computed in $t \in [t^n, t^{n+1}]$, takes effect only within $[t^n, t^{n+1}]$, and can be discarded when we move to the next step, where $t \in [t^{n+1}, t^{n+2}]$. On the other hand, in the gauge method, the gauge variables are defined globally over the whole time domain. In this sense, continuous projection method can be regarded as a local or adaptive gauge method. The solution procedures of both the continuous projection method and the gauge method can be illustrated in Fig. 1, in which three solid curves $\boldsymbol{u}$, $\tilde{\boldsymbol{u}}$ and $\boldsymbol{a}$ denote exact velocity, velocity obtained using the projection method and the gauge variable of the gauge method, respectively. It can be seen that, at every time step, for example at $t = t^n$, we have in fact two intermediate velocity fields and two potentials: the overbared $\boldsymbol{u}^*$ and ϕ, $(\bar{\boldsymbol{u}}^*)^n$ and $\bar{\phi}^n$, are the solutions of the continuous projection method when $t \in [t^{n-1}, t^n]$; and the underlined $\boldsymbol{u}^*$ and ϕ, $(\underline{\boldsymbol{u}}^*)^n$ and $\underline{\phi}^n$, are the initial conditions of the continuous projection method when $t \in [t^n, t^{n+1}]$, which satisfy $(\underline{\boldsymbol{u}}^*)^n = \underline{\tilde{\boldsymbol{u}}}^n$ and $\nabla \underline{\phi}^n = 0$, respectively. It is clear that, unlike the auxiliary field $\boldsymbol{a}$ in gauge method, $\boldsymbol{u}^*$ never deviates much from the divergence-free velocity field in the continuous projection method.

The second and less important difference between these two methods is that the gauge method is a pressure-free method in which the pressure is not needed in the solution procedure. However, the continuous projection method can be both pressure-free when $q = 0$ or in incremental-pressure form when q approximating the pressure to a certain degree.

3. The fully second order accurate continuous projection methods

3.1. The LTE analysis of the continuous projection method

At time interval between t^n and t^{n+1}, we denote the exact solutions of Eqs. (2) and (3) as $\boldsymbol{u}^\varepsilon = \boldsymbol{u}(t^n + \varepsilon)$ and $p^\varepsilon = p(t^n + \varepsilon)$, and the solutions of continuous projection methods as $\tilde{\boldsymbol{u}}^\varepsilon = \tilde{\boldsymbol{u}}(t^n + \varepsilon)$ and $\tilde{p}^\varepsilon = \tilde{p}(t^n + \varepsilon)$, where $0 \leqslant \varepsilon \leqslant \Delta t = t^{n+1} - t^n$. Setting

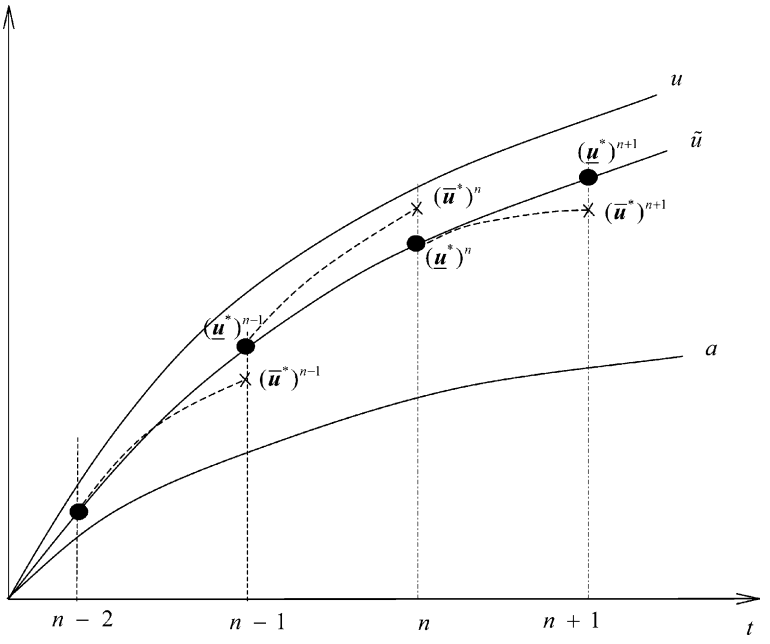

Fig. 1. The diagram showing the solution procedures of the continuous projection method and the gauge method.

$$\tilde{\boldsymbol{u}}(t_n) = \boldsymbol{u}(t_n), \quad \tilde{p}(t_n) = p(t_n),$$

the local truncation errors of velocity and pressure can be defined, respectively, by

$$e_{\boldsymbol{u}} = \boldsymbol{u}^{\varepsilon} - \tilde{\boldsymbol{u}}^{\varepsilon} = \boldsymbol{u}^{\varepsilon} - \boldsymbol{u}^{*,\varepsilon} + \nabla\phi^{\varepsilon}, \tag{15}$$

and

$$e_p = p^{\varepsilon} - \tilde{p}^{\varepsilon} = p^{\varepsilon} - q^{\varepsilon} - \frac{\partial\phi^{\varepsilon}}{\partial t} + \upsilon\Delta\phi^{\varepsilon}. \tag{16}$$

Assuming the solutions are smooth enough, the Taylor series expansion can be applied to $\boldsymbol{u}^{\varepsilon}$, p^{ε} and $\boldsymbol{u}^{*,\varepsilon}$ at $t = t^n$:

$$\boldsymbol{u}^{\varepsilon} = \boldsymbol{u}^n + \varepsilon\dot{\boldsymbol{u}}^n + \frac{\varepsilon^2}{2}\ddot{\boldsymbol{u}}^n + \mathrm{O}(\varepsilon^3), \tag{17}$$

$$p^{\varepsilon} = p^n + \varepsilon\dot{p}^n + \mathrm{O}(\varepsilon^2), \tag{18}$$

$$\boldsymbol{u}^{*,\varepsilon} = (\boldsymbol{u}^*)^n + \varepsilon(\dot{\boldsymbol{u}}^*)^n + \frac{\varepsilon^2}{2}(\ddot{\boldsymbol{u}}^*)^n + \mathrm{O}(\varepsilon^3). \tag{19}$$

According to Eq. (2), $\dot{\boldsymbol{u}}^n$ and $\ddot{\boldsymbol{u}}^n$ can be reformulated as

$$\dot{\boldsymbol{u}}^n = \upsilon\Delta\boldsymbol{u}^n - \nabla p^n + \boldsymbol{f}^n,$$

$$\ddot{\boldsymbol{u}}^n = \upsilon^2\Delta^2\boldsymbol{u}^n - \upsilon\Delta(\nabla p^n - \boldsymbol{f}^n) - \nabla\dot{p}^n + \dot{\boldsymbol{f}}^n.$$

Inserting $\dot{\boldsymbol{u}}^n$ and $\ddot{\boldsymbol{u}}^n$ into Eq. (17), we can get

$$\boldsymbol{u}^{\varepsilon} = \left(1 + \varepsilon\upsilon\Delta + \varepsilon^2\frac{\upsilon^2}{2}\Delta^2\right)\boldsymbol{u}^n - \varepsilon\left(1 + \frac{\varepsilon\upsilon}{2}\Delta\right)(\nabla p^n - \boldsymbol{f}^n) - \frac{\varepsilon^2}{2}(\nabla\dot{p}^n - \dot{\boldsymbol{f}}^n) + \mathrm{O}(\varepsilon^3). \tag{20}$$

Similar to $\dot{\boldsymbol{u}}^n$ and $\ddot{\boldsymbol{u}}^n$, variables $(\boldsymbol{u}^*)^n$, $(\dot{\boldsymbol{u}}^*)^n$ and $(\ddot{\boldsymbol{u}}^*)^n$ can be written as

$$(\boldsymbol{u}^*)^n = \boldsymbol{u}^n,$$

$$(\dot{\boldsymbol{u}}^*)^n = \upsilon\Delta\boldsymbol{u}^n - \nabla q^n + \boldsymbol{f}^n,$$

$$(\ddot{\boldsymbol{u}}^*)^n = \upsilon^2\Delta^2\boldsymbol{u}^n - \upsilon\Delta(\nabla q^n - \boldsymbol{f}^n) - \nabla\dot{q}^n + \dot{\boldsymbol{f}}^n,$$

respectively. After substituting the corresponding terms in Eq. (19) by the equations above, the intermediate velocity can be estimated by

$$\boldsymbol{u}^{*,\varepsilon} = \left(1 + \varepsilon\upsilon\Delta + \varepsilon^2\frac{\upsilon^2}{2}\Delta^2\right)\boldsymbol{u}^n - \varepsilon\left(1 + \frac{\varepsilon\upsilon}{2}\Delta\right)(\nabla q^n - \boldsymbol{f}^n) - \frac{\varepsilon^2}{2}(\nabla\dot{q}^n - \dot{\boldsymbol{f}}^n) + \mathrm{O}(\varepsilon^3). \tag{21}$$

Since q^{ε} is an estimation of p^{ε}, it can be expanded at $t = t^n$ in the following form:

$$q^{\varepsilon} = \alpha_0 p^n + \alpha_1\varepsilon\dot{p}^n + \mathrm{O}(\varepsilon^2), \tag{22}$$

where α_i are coefficients corresponding to a specific choice of q^{ε}. It is apparent that

$$q^n = \alpha_0 p^n, \quad \dot{q}^n = \alpha_1\dot{p}^n.$$

Inserting these terms into Eq. (21), we get

$$\boldsymbol{u}^{*,\varepsilon} = \left(1 + \varepsilon\upsilon\Delta + \varepsilon^2\frac{\upsilon^2}{2}\Delta^2\right)\boldsymbol{u}^n - \varepsilon\left(1 + \frac{\varepsilon\upsilon}{2}\Delta\right)(\alpha_0\nabla p^n - \boldsymbol{f}^n) - \frac{\varepsilon^2}{2}(\alpha_1\nabla\dot{p}^n - \dot{\boldsymbol{f}}^n) + \mathrm{O}(\varepsilon^3). \tag{23}$$

Using Eqs. (20)–(23), the LTEs defined in Eqs. (15) and (16) can be expressed by

$$e_{\boldsymbol{u}} = \varepsilon(\alpha_0 - 1)\nabla p^n + \frac{\varepsilon^2}{2}\left[(\alpha_0 - 1)\upsilon\Delta\nabla p^n + (\alpha_1 - 1)\nabla\dot{p}^n\right] + \nabla\phi^\varepsilon + \mathrm{O}(\varepsilon^3), \tag{24}$$

$$e_p = (1 - \alpha_0)p^n + \varepsilon(1 - \alpha_1)\dot{p}^n + \upsilon\Delta\phi - \frac{\partial\phi^\varepsilon}{\partial\varepsilon} + \mathrm{O}(\varepsilon^2). \tag{25}$$

It is clear that a rigorous LTE analysis is possible only after an estimation of ϕ^ε is available. Substituting Eq. (23) into Eq. (9), and taking Eqs. (8) and (20) into consideration, we arrive at

$$\nabla\cdot\nabla\phi^\varepsilon = \varepsilon\nabla\cdot\left\{(1 - \alpha_0)\nabla p^n + \frac{\varepsilon}{2}\left[(1 - \alpha_0)\upsilon\Delta\nabla p^n + (1 - \alpha_1)\nabla\dot{p}^n\right]\right\} + \mathrm{O}(\varepsilon^3). \tag{26}$$

The boundary condition is

$$\frac{\partial\phi^\varepsilon_{\mathrm{b}}}{\partial n} = \frac{\partial\psi^\varepsilon}{\partial n}. \tag{27}$$

For arbitrary ψ^ε in Eq. (27), it is difficult to get a close form estimation of ϕ^ε according to Eq. (26). Hence, in order to get a rigorous LTE estimation, ψ^ε must be specified appropriately. The most obvious choice is

$$\nabla\psi^\varepsilon = \varepsilon\left\{(1 - \alpha_0)\nabla p^n + \frac{\varepsilon}{2}\left[(1 - \alpha_0)\upsilon\Delta\nabla p^n + (1 - \alpha_1)\nabla\dot{p}^n\right]\right\}_{\mathrm{b}} + \mathrm{O}(\varepsilon^3).$$

Then the boundary condition of Eq. (11) will be expressed as

$$\boldsymbol{n}\cdot\nabla\phi^\varepsilon_{\mathrm{b}} = \boldsymbol{n}\cdot\nabla\psi^\varepsilon = \boldsymbol{n}\cdot\left\{\varepsilon(1 - \alpha_0)\nabla p^n + \frac{\varepsilon^2}{2}\left[(1 - \alpha_0)\upsilon\Delta\nabla p^n + (1 - \alpha_1)\nabla\dot{p}^n\right]\right\}_{\mathrm{b}} + \mathrm{O}(\varepsilon^3). \tag{28}$$

Considering Eqs. (26) and (28), ϕ^ε can be expressed in the following form (omitting the constant):

$$\phi^\varepsilon = \varepsilon(1 - \alpha_0)p^n + \frac{\varepsilon^2}{2}\left[(1 - \alpha_0)\upsilon\Delta p^n + (1 - \alpha_1)\dot{p}^n\right] + \mathrm{O}(\varepsilon^3). \tag{29}$$

Using Eqs. (15), (16) and (29), we get the LTEs of velocity and pressure for the continuous projection methods

$$e_{\boldsymbol{u}} = \mathrm{O}(\varepsilon^3), e_p = \mathrm{O}(\varepsilon^2),$$

which are sufficient for the continuous projection methods to be second order accurate in time for both the velocity and the pressure. This fact leads to the following theorem.

Theorem. *If the guessed pressure is given by*

$$q^\varepsilon = \alpha_0 p^n + \alpha_1\varepsilon\dot{p}^n + \mathrm{O}(\varepsilon^2),$$

then the sufficient condition for the continuous projection methods described in Eqs. (4), (7), (9) *and* (14) *to be second order accurate in time is*

$$\nabla\psi^{\varepsilon} = \varepsilon\left\{(1-\alpha_0)\nabla p^n + \frac{\varepsilon}{2}\left[(1-\alpha_0)\upsilon\Delta\nabla p^n + (1-\alpha_1)\nabla\dot{p}^n\right]\right\}_{\mathrm{b}} + \mathrm{O}(\varepsilon^3) \tag{30}$$

in which α_i $(i = 0, 1)$ *can be chosen arbitrarily.*

We have therefore obtained a class of fully second order continuous projection schemes in which the artificial boundary conditions for $\boldsymbol{u}^{*,\varepsilon}$ are

$$\boldsymbol{u}_{\mathrm{b}}^{*,\varepsilon} = \boldsymbol{w}^{\varepsilon} + \varepsilon\left\{(1-\alpha_0)\nabla p^n + \frac{\varepsilon}{2}\left[(1-\alpha_0)\upsilon\Delta\nabla p^n + (1-\alpha_1)\nabla\dot{p}^n\right]\right\}_{\mathrm{b}} + \mathrm{O}(\varepsilon^3). \tag{31}$$

3.2. The analysis of the second order continuous projection method

The governing equations and boundary conditions of the fully second order continuous projection method can be summarized as follows:

$$\frac{\partial\boldsymbol{u}^*}{\partial\varepsilon} + \alpha_0 p^n + \alpha_1\varepsilon\dot{p}^n - \upsilon\Delta\boldsymbol{u}^* = \boldsymbol{f}, \tag{32}$$

$$\boldsymbol{u}_{\mathrm{b}}^* = \boldsymbol{w} + \varepsilon\left\{(1-\alpha_0)\nabla p^n + \frac{\varepsilon}{2}\left[(1-\alpha_0)\upsilon\Delta\nabla p^n + (1-\alpha_1)\nabla\dot{p}^n\right]\right\}_{\mathrm{b}}, \tag{33}$$

$$\nabla^2\phi = \nabla\cdot\boldsymbol{u}^*, \tag{34}$$

$$\frac{\partial\phi_{\mathrm{b}}}{\partial n} = \left(\frac{\partial\left\{(1-\alpha_0)\varepsilon p^n + \frac{\varepsilon^2}{2}\left[(1-\alpha_0)\upsilon\Delta p^n + (1-\alpha_1)\dot{p}^n\right]\right\}}{\partial n}\right)_{\mathrm{b}}, \tag{35}$$

$$\tilde{\boldsymbol{u}} = \boldsymbol{u}^* - \nabla\phi, \tag{36}$$

$$\tilde{p} = \alpha_0 p^n + \alpha_1\varepsilon\dot{p}^n + \frac{\partial\phi}{\partial\varepsilon} - \upsilon\Delta\phi. \tag{37}$$

Because α_0 and α_1 can be chosen arbitrarily, the equations above constitute a class of fully second order accurate continuous projection schemes. When $\alpha_0 = 0$ and $\alpha_1 = 0$, the projection method is in the pressure-free form; otherwise, the projection method is in incremental-pressure form. An important case can be obtained if we set $\alpha_0 = 1$ and $\alpha_1 = 1$, which is called the second order incremental pressure projection method in the present paper. In this case, the artificial boundary conditions become very simple:

$$\boldsymbol{u}_{\mathrm{b}}^* = \boldsymbol{w}, \tag{38}$$

$$\frac{\partial\phi_{\mathrm{b}}}{\partial n} = 0. \tag{39}$$

Except this special case, the artificial boundary conditions are rather complex and related to the spatial and/or temporal derivatives of the pressure at time t^n.

It is well known that the boundary conditions and their discretization procedures have important influence on the stability property of the numerical solution schemes. In this regard, the simpler boundary conditions, such as Eqs. (38) and (39), are preferred because they will not adversely affect the stability of the numerical scheme if they are properly discretized. For the continuous projection method,

Eqs. (32)–(37), the artificial boundary conditions, can be greatly simplified using simple variable transformations. Define

$$\hat{\boldsymbol{u}}^* = \boldsymbol{u}^* - \varepsilon\left\{(1-\alpha_0)\nabla p^n + \frac{\varepsilon}{2}\left[(1-\alpha_0)\upsilon\Delta\nabla p^n + (1-\alpha_1)\nabla\dot{p}^n\right]\right\}$$

and

$$\hat{\phi} = \phi - \varepsilon\left\{(1-\alpha_0)p^n + \frac{\varepsilon}{2}\left[(1-\alpha_0)\upsilon\Delta p^n + (1-\alpha_1)\dot{p}^n\right]\right\}.$$

Eqs. (32)–(37) can be rewritten as

$$\frac{\partial\hat{\boldsymbol{u}}^*}{\partial\varepsilon} + \nabla(p^n + \varepsilon\dot{p}^n) - \upsilon\Delta\hat{\boldsymbol{u}}^* = \boldsymbol{f} + \frac{\varepsilon^2\upsilon}{2}\Delta\left[(1-\alpha_0)\upsilon\Delta\nabla p^n + (1-\alpha_1)\nabla\dot{p}^n\right], \tag{40}$$

$$\hat{\boldsymbol{u}}^*_{\mathrm{b}} = \boldsymbol{w}, \tag{41}$$

$$\nabla^2\hat{\phi} = \nabla\cdot\hat{\boldsymbol{u}}^*, \tag{42}$$

$$\left.\frac{\partial\hat{\phi}}{\partial n}\right|_{\mathrm{b}} = 0, \tag{43}$$

$$\tilde{\boldsymbol{u}} = \hat{\boldsymbol{u}}^* - \nabla\hat{\phi}, \tag{44}$$

$$\tilde{p} = p^n + \varepsilon\dot{p}^n + \frac{\partial\hat{\phi}}{\partial\varepsilon} - \upsilon\Delta\hat{\phi} + \frac{\varepsilon^2\upsilon}{2}\Delta\left[(1-\alpha_0)\upsilon\Delta p^n + (1-\alpha_1)\dot{p}^n\right]. \tag{45}$$

Neglecting the second order ($O(\varepsilon^2)$) terms, Eqs. (40)–(45) are identical to the second order incremental pressure projection method ($\alpha_0 = 1$ and $\alpha_1 = 1$ in Eqs. (32)–(37) mentioned above. Therefore, we will consider the second order incremental pressure projection method only in the following sections without loss of generality.

4. The second order accurate discrete projection method

4.1. The second order accurate discrete projection method

The continuous second order incremental pressure projection method can be derived by setting $\alpha_0 = 1$ and $\alpha_1 = 1$ in Eqs. (32)–(37):

$$\frac{\partial\boldsymbol{u}^*}{\partial\varepsilon} + \nabla(p^n + \varepsilon\dot{p}^n) - \upsilon\Delta\boldsymbol{u}^* = \boldsymbol{f}, \tag{46}$$

$$\boldsymbol{u}^*_{\mathrm{b}} = \boldsymbol{w}, \tag{47}$$

$$\nabla^2\phi = \nabla\cdot\boldsymbol{u}^*, \tag{48}$$

$$\frac{\partial \phi_{\mathrm{b}}}{\partial n} = 0, \tag{49}$$

$$\tilde{\boldsymbol{u}} = \boldsymbol{u}^* - \nabla\phi, \tag{50}$$

$$\tilde{p} = p^n + \varepsilon \dot{p}^n + \frac{\partial \phi}{\partial \varepsilon} - \upsilon \Delta\phi. \tag{51}$$

Because these equations are the second order approximation of the Stokes equations, any second order discretiztions of this set of equations will result in a second order numerical scheme for solving the original Stokes equations. In the present paper, this set of equations is discretized in time using the Crank–Nicholson scheme at $t^{n+1/2}$. The spatial derivatives are discretized using the second order central difference schemes. The resulting finite difference schemes are:

$$\frac{(\boldsymbol{u}^*)^{n+1} - \tilde{\boldsymbol{u}}^n}{\Delta t} + Gq^{n+1/2} - \frac{\upsilon}{2}\boldsymbol{L}[(\boldsymbol{u}^*)^{n+1} + \tilde{\boldsymbol{u}}^n] = \boldsymbol{f}^{n+1/2}, \tag{52}$$

$$(\boldsymbol{u}^*_{\mathrm{b}})^{n+1} = \boldsymbol{w}^{n+1}, \tag{53}$$

$$L\phi^{n+1} = \boldsymbol{D}(\boldsymbol{u}^*)^{n+1}, \tag{54}$$

$$\frac{\delta \phi^{n+1}_{\mathrm{b}}}{\delta n} = 0, \tag{55}$$

$$\tilde{\boldsymbol{u}}^{n+1} = (\boldsymbol{u}^*)^{n+1} - \boldsymbol{G}\phi^{n+1}, \tag{56}$$

$$\tilde{p}^{n+1/2} = q^{n+1/2} + \frac{\phi^{n+1} - \phi^n}{\Delta t} - \frac{\upsilon}{2}\boldsymbol{L}(\phi^{n+1} + \phi^n), \tag{57}$$

where $\boldsymbol{D}$, $\boldsymbol{G}$ and $\boldsymbol{L}$ are the second order accurate discrete divergence, gradient and Laplacian operators, respectively, and $q^{n+1/2}$ is a second order approximation of $p^n + \frac{\Delta t}{2}\dot{p}^n$, which can be evaluated by

$$q^{n+1/2} = 2\tilde{p}^{n-1/2} - \tilde{p}^{n-3/2}. \tag{58}$$

In deriving Eq. (52), the relation $(\boldsymbol{u}^*)^n = \tilde{\boldsymbol{u}}^n$ has been used. Using the notation introduced in Section 2, Eq. (57) is in fact

$$\tilde{p}^{n+1/2} = q^{n+1/2} + \frac{\bar{\phi}^{n+1} - \underline{\phi}^n}{\Delta t} - \frac{\upsilon}{2}\boldsymbol{L}(\bar{\phi}^{n+1} + \underline{\phi}^n).$$

Since $\nabla\underline{\phi}^n = (\boldsymbol{u}^*)^n - \tilde{\boldsymbol{u}}^n = 0$, we set $\underline{\phi}^n = 0$ without loss of generality. Therefore, Eq. (57) can be rewritten as

$$\tilde{p}^{n+1/2} = q^{n+1/2} + \frac{\phi^{n+1}}{\Delta t} - \frac{\upsilon}{2}\boldsymbol{L}(\phi^{n+1}). \tag{59}$$

The boundary condition (55) is implemented by setting suitable values on ghost grid points. For example, at the left boundary denoted by (1/2,j) for a two-dimensional rectangular domain, ϕ at ghost grid point (0,j) can be set to be $\phi_{0,j} = \phi_{1,j}$.

Remark. The discrete projection method in this paper is identical to Pm II in [4] if Eq. (58) is replaced by $q^{n+1/2} = \tilde{p}^{n-1/2}$. It is clear that Pm II does not satisfy the sufficient condition derived in Section 3.1. The temporal accuracy of Pm II has been studied in [4,17]. In the periodic semi-infinite strip $\Omega = [0, \infty) \times [-\pi, \pi]$, for $t \geqslant 0$, Brown et al. have shown that the Pm II is temporally second order accurate by normal mode analysis. In general domains, however, Guermond and Shen [17] have found that the pressure field computed by Pm II is at best temporally 3/2-order accurate. On the other hand, the LTE analysis in Section 3.1 shows that the present projection method is temporally second order accurate regardless the shape of the computational domain. In Section 5, we will compare the numerical results obtained by the present projection method and Pm II, which show that while the present method is temporally fully second order accurate, the convergence rate of pressure calculated by Pm II is depended on the type of boundary conditions. When Dirichlet condition is used on all boundaries, the computed convergence rate of pressure is around 1.6 which is in accordance with [17].

4.2. Remarks on the stability of the present projection method

In [30], Shen showed that similar second order incremental pressure projection method (the projection-3 scheme in [13,14]) is unconditionally unstable. However, in his analysis, the pressure updating scheme is different from the present one. The consistent pressure updating formulation, Eq. (14) or (59), turns out to have favorable effect on the stability property of the numerical scheme, which have been observed in higher order velocity correction projection schemes [18]. In this subsection, we will show that the present second order projection scheme can be stable using the same technique of Shen.

Using the notation introduced in Section 2, Eq. (52), can be written as

$$\frac{(\bar{\boldsymbol{u}}^*)^{n+1} - (\bar{\boldsymbol{u}}^*)^n}{\Delta t} + Gq^{n+1/2} + \frac{G\phi^n}{\Delta t} - \frac{\upsilon}{2}\boldsymbol{L}[(\bar{\boldsymbol{u}}^*)^{n+1} + (\bar{\boldsymbol{u}}^*)^n - G\phi^n] = \boldsymbol{f}^{n+1/2}.$$

Considering Eq. (59), we have

$$\frac{(\bar{\boldsymbol{u}}^*)^{n+1} - (\bar{\boldsymbol{u}}^*)^n}{\Delta t} + \boldsymbol{G}\tilde{p}^{n+1/2} - \frac{\boldsymbol{G}(\phi^{n+1} - \phi^n)}{\Delta t} + \frac{\upsilon}{2}(\boldsymbol{GL}\phi^{n+1} + \boldsymbol{LG}\phi^n) - \frac{\upsilon}{2}\boldsymbol{L}[(\bar{\boldsymbol{u}}^*)^{n+1} + (\bar{\boldsymbol{u}}^*)^n] = \boldsymbol{f}^{n+1/2}. \tag{60}$$

The combination of Eqs. (59) and (58) gives

$$\tilde{p}^{n+1/2} - 2\tilde{p}^{n-1/2} + \tilde{p}^{n-3/2} = \frac{\phi^{n+1}}{\Delta t} - \frac{\upsilon}{2}\boldsymbol{L}(\phi^{n+1}). \tag{61}$$

Eqs. (60) and (61), together with the Poisson equation

$$\boldsymbol{L}\phi^{n+1} = \boldsymbol{D}(\bar{\boldsymbol{u}}^*)^{n+1}, \tag{62}$$

form a closed set of finite difference equations.

Considering $\tau \sim \Delta t \to 0,\ \Delta x \to 0$, the following singularly perturbed equations in continuous form can be obtained (note $\boldsymbol{GL} = \boldsymbol{LG}$ when $\Delta x \to 0$):

$$\bar{\boldsymbol{u}}_t^* + \nabla p - \nabla(\phi_t - \upsilon\Delta\phi) - \upsilon\Delta\bar{\boldsymbol{u}}^* = \boldsymbol{f}, \tag{63}$$

$$\tau^2 p_{tt} = \phi_t - \upsilon\Delta\phi, \tag{64}$$

$$\Delta\phi = \nabla \cdot \bar{\boldsymbol{u}}^*. \tag{65}$$

Eliminating $\bar{u}^*$, p from Eqs. (63)–(65), we have

$$\Delta\phi_t - \upsilon\Delta^2\phi = \tau^2\nabla\cdot\boldsymbol{f}_{tt} \tag{66}$$

with boundary condition $\partial\phi/\partial n = 0$.

Let $\{\lambda_n, \phi_n\}$ be the eigenpair of the Laplacian operator with homogeneous Neumann boundary conditions, i.e.

$$-\Delta\phi_n = \lambda_n\phi_n, \quad \left(\frac{\partial\phi_n}{\partial n}\right)_{\mathrm{b}} = 0 \tag{67}$$

with $0 = \lambda_0 < \lambda_1 < \cdots < \cdots + \infty$. We can then expand ϕ and $\nabla\cdot\boldsymbol{f}_{tt}$ of Eq. (66) by using the eigenfunctions

$$\phi = \sum_{n=0}^{\infty} c_n(t)\phi_n, \quad \nabla\cdot\boldsymbol{f}_{tt} = \sum_{n=0}^{\infty} d_n(t)\phi_n. \tag{68}$$

Substituting Eq. (68) into Eq. (66), we obtain

$$\dot{c}_n(t) + \upsilon\lambda_n c_n(t) = -\frac{\tau^2}{\lambda_n} d_n(t) \quad \forall n \geqslant 1. \tag{69}$$

The general solution of Eq. (69) is of the form

$$c_n(t) = C\mathrm{e}^{-\upsilon\lambda_n t}. \tag{70}$$

We can then conclude that ϕ is uniformly bounded for $t \in [0, +\infty)$ and therefore the singularly perturbed system is stable.

It should be noted that this analysis cannot be regarded as a rigorous proof of the stability of the discrete projection scheme because only the continuous singularly perturbed equations are considered. However, it does indicate that it possible to construct a stable discrete second order projection scheme. The numerical experiments presented in Section 5 show that the numerical scheme (Eqs. (52)–(58)) is stable under CFL-like conditions.

5. Numerical tests

In this section, we will apply the proposed projection scheme to numerically simulate four incompressible flow test cases. It should be noted that in this section, the governing equations are the incompressible N–S equations instead of the Stokes equations. The convection terms are discretized spatially with the second order central difference scheme and temporally with the Adams–Barshforth scheme to ensure overall second order accuracy. A staggered grid arrangement is used to achieve the grid-level coupling in the pressure field and to remove the odd–even decoupling.

For a temporally rth order and spatially sth order scheme, the numerical solution can be interpreted as

$$\eta^n_{i,j} = \eta(x_i, y_j, t^n) + \beta^n_{i,j}(\Delta t)^r + \gamma^n_{i,j}(\Delta x)^s + \delta,$$

where $\eta^n_{i,j}$ and $\eta(x_i, y_j, t^n)$ are the numerical and analytical solutions, respectively. $\beta^n_{i,j}(\Delta t)^r$ and $\gamma^n_{i,j}(\Delta x)^s$ are corresponding to the errors due to temporal and spatial discretizations, and δ is the round-off error which is considered to be much smaller than the discretization errors. To check the temporal accuracy, we first carry out the computation using a very small time step so that the numerical solution can be approximated by

$$\tilde{\eta}^n_{i,j} \approx \eta(x_i, y_j, t^n) + \gamma^n_{i,j}(\Delta x)^s + \delta,$$

where $\tilde{\eta}^n_{i,j}$ is called the reference solution. Then the numerical solutions $\eta^n_{i,j}$ are computed with various computational time steps on the same grid. It is easy to show

$$\|e_\eta\| = \|\eta^n - \tilde{\eta}^n\| \sim (\Delta t)^r,$$

where e_η is called the temporal error in this paper. Therefore, the slope of the $\|e_\eta\| \sim \Delta t$ curve in double logarithm scale can be used to determine the convergence rate as well as the order of temporal accuracy of the numerical method.

For convenience, we denote the discrete projection method proposed in Section 4.1 by DPM. The computational results of DPM will be compared with those of Pm II [4] in this section.

5.1. Case 1: doubly periodic shear layer

This test case is taken from [23]. It consists of two jets in a doubly periodic geometry to which a sinusoidal perturbation perpendicular to the orientation of the shear layers is imposed at the lowest wave number supported by the computational mesh. In the absence of any additional perturbations, each of the shear layers rolls up in a single vortex as the flow evolves. In the periodical two-dimensional computational domain of size $(0,1) \times (0,1)$, the following velocity fields are generated as initial condition:

$$u = \begin{cases} \tanh(\lambda(y - 0.25)), & y \leqslant 0.5, \\ \tanh(\lambda(0.75 - y)), & y > 0.5, \end{cases}$$

$$v = \gamma \sin(2\pi(x + 0.25)).$$

We first consider the "thick" shear layer case with the width parameter λ being set to 30. The strength coefficient γ is 0.05 and the Reynolds number is 10,000. The temporal errors of the computed velocity and pressure in both the 2- and ∞-norm at $t = 1$ are reported in Fig. 2. The second order convergence rate is observed in both the 2- and the ∞-norm. The temporal errors obtained using Pm II are also shown in Fig. 2. We note that when doubly periodic boundary conditions are used, the computational results of DPM and Pm II are quite similar. For the "thin" shear layer case with λ being 80, Fig. 3 presents the

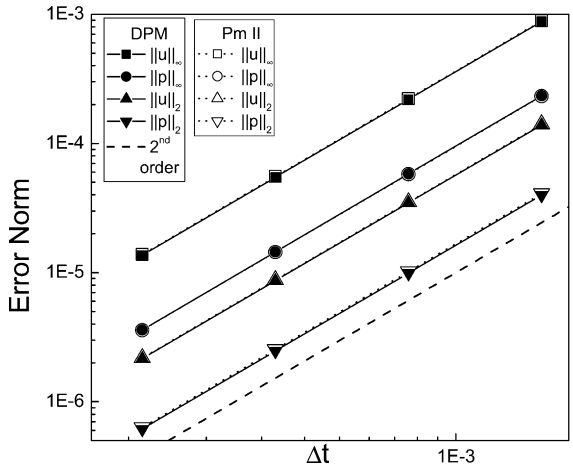

Fig. 2. Convergence rates of DPM and Pm II at $t = 1$ on 128×128 grids for the "thick" shear layer case.

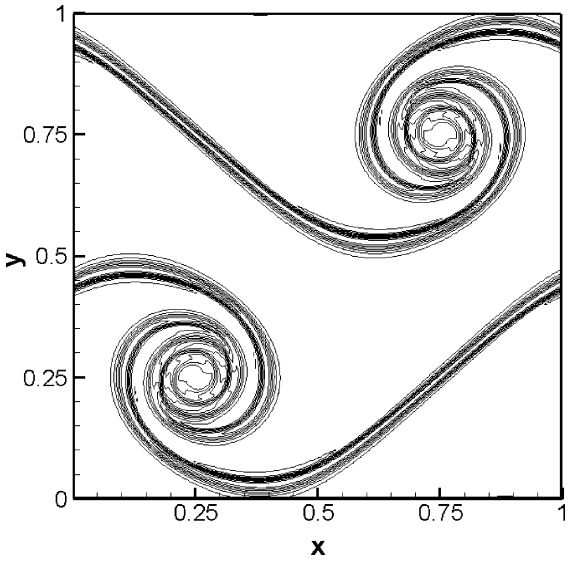

Fig. 3. Contour plots of vorticity (30 isolines) for the "thin" shear layer case, when $Re = 10{,}000$ and $t = 1$. Computational results are obtained by DMP with $\Delta t/h = 0.25$ on 256×256 grids.

calculated vorticity field at time $t = 1$ with $\Delta t/h = 0.25$ on a 256×256 grid, which is similar to the results in [23].

5.2. Case 2: the forced flow problem 1

In this test case [4], the fluid flows in a channel with periodic boundary conditions in the x-direction. A no-slip condition is prescribed at $y = 0$, while a non-trivial slip condition is specified at $y = 1$. The N–S equations are augmented with a forcing term in order that the solution is

$$u = \cos(2\pi(x - \omega(t)))(3y^2 - y),$$

$$v = 2\pi \sin(2\pi(x - \omega(t)))y^2(y - 1),$$

$$p = -\frac{\dot{\omega}(t)}{2\pi} \sin(2\pi(x - \omega(t)))(\sin(2\pi y) - 2\pi y + \pi) + \upsilon \cos(2\pi(x - \omega(t)))(\sin(2\pi y)2\pi y + \pi),$$

where $\omega(t) = 1 + \sin(2\pi t^2)$, and the viscosity is set to $\upsilon = 1$. Errors are calculated at the time $t = 0.5$ on 64×64 grids.

Fig. 4 displays the errors of the computed velocity and pressure in both the 2- and ∞-norm at $t = 0.5$. The second order convergence rate is observed for both DPM and Pm II. The error field calculated by DPM and Pm II for both the velocity and the pressure with $\Delta t/h = 0.5$ are shown in Figs. 5 and 6, respectively. No numerical boundary layer is observed for both the velocity and the pressure in the computational results of DPM. We note when the periodic boundary condition is applied in one direction and Dirichlet boundary conditions are used on other boundaries, both DPM and Pm II achieve the second order rate of convergence. However, the errors calculated by DPM are significantly smaller than those by Pm II especially near the boundaries using Dirichlet boundary conditions ($y = 0$ and $y = 1$).

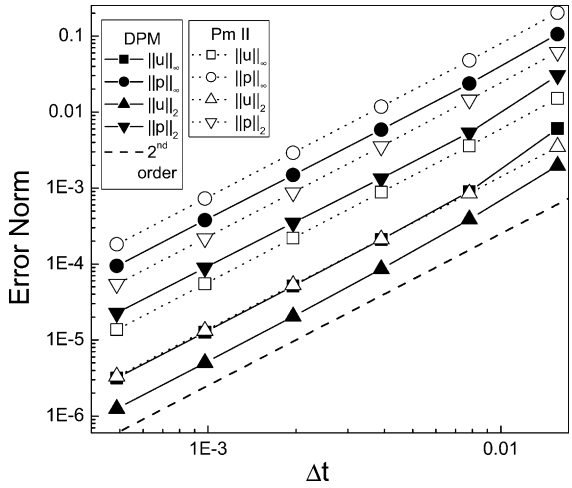

Fig. 4. Convergence rates of DPM and Pm II at $t = 0.5$ on 64×64 grids when computing case 2.

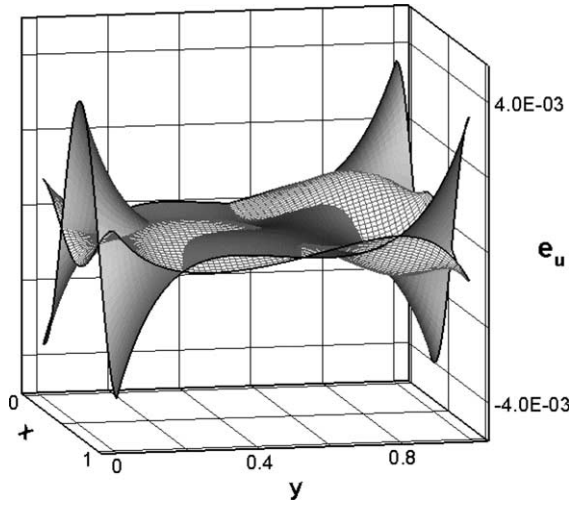

Fig. 5. The field of e_u for case 2 at $t = 0.5$. The computational result obtained by DMP is denoted by the surface with mesh, and is compared to the results obtained by Pm II denoted by the shaded surface on 64×64 grids with $\Delta t/h = 0.5$.

5.3. Case 3: the forced flow problem 2

The third test case is also a forced flow problem [17]. The computational domain is $(0,1) \times (0,1)$. The source term is added to the N–S equations so that the exact solution is

$$u = \pi \sin(t) \sin^2(2\pi x) \sin(2\pi y),$$

$$v = -\pi \sin(t) \sin(2\pi x) \sin^2(2\pi y),$$

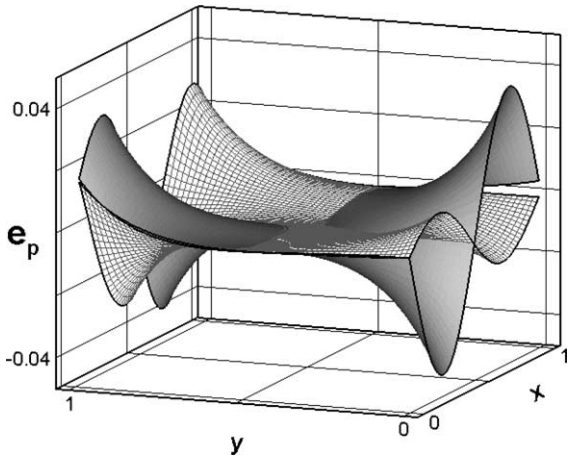

Fig. 6. The field of e_p for case 2 at $t = 0.5$. The computational result obtained by DPM is denoted by the surface with mesh, and is compared to the results obtained by PM II denoted by the shaded surface on 64×64 grids with $\Delta t/h = 0.5$.

$$p = \sin(t)\cos(\pi x)\cos(\pi y).$$

Dirichlet boundary conditions are applied at all boundaries. The viscosity is $\upsilon = 1$. The errors are calculated at $t = 1$ on the same grids as in case 2.

In Fig. 7, we show the errors of the velocity and the pressure in both the 2- and the ∞-norm at $t = 1$ using different time steps. The velocity fields again exhibit the second order convergence rates for both DPM and Pm II in the 2-norm as well as the ∞-norm. In the present case, the pressure field achieves surprisingly 2.5th-order rate of convergence using DPM, while the convergence rate of Pm II is around 1.6, which is in accordance with [17].

The temporal error fields of the velocity and pressure computed using DPM and Pm II on 64×64 grids are plotted in Figs. 8 and 9, respectively. Large differences in velocity errors between the numerical results

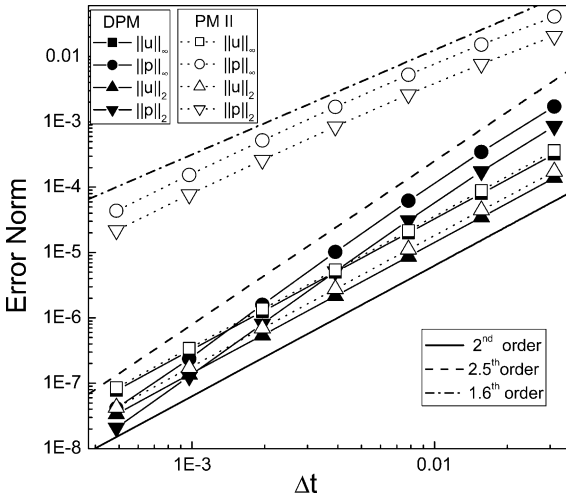

Fig. 7. Convergence rates of DPM and Pm II at $t = 1.0$ on 64×64 grids when computing case 3.

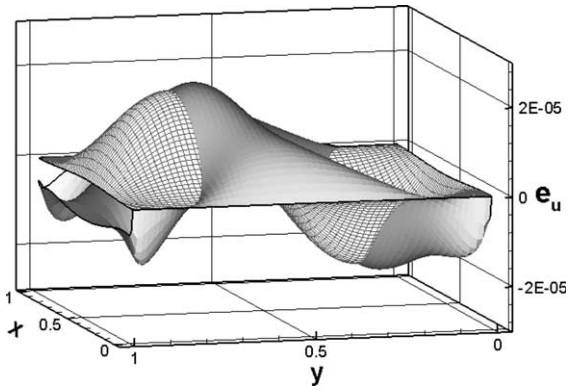

Fig. 8. The field of e_u for case 3 at $t = 1$. The computational result obtained by DMP is denoted by the surface with mesh, and is compared to the results obtained by Pm II denoted by the shaded surface on 64×64 grids with $\Delta t/h = 0.5$.

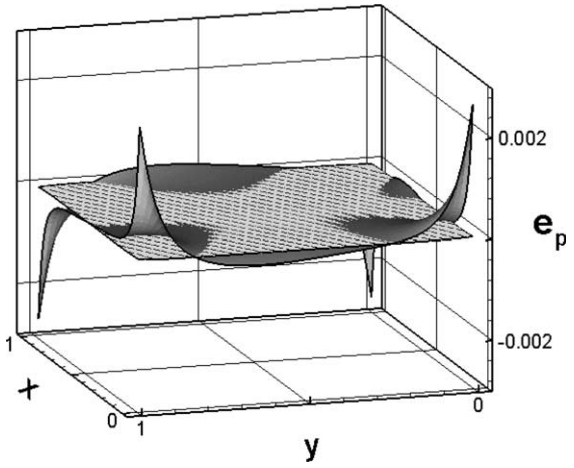

Fig. 9. The field of e_p for case 3 at $t = 1$. The computational result obtained by DPM is denoted by the surface with mesh, and is compared to the results obtained by Pm II denoted by the shaded surface on 64×64 grids with $\Delta t/h = 0.5$.

of these two schemes appear near the boundaries ($y = 0$ and $y = 1$ for u-component in Fig. 8; $x = 0$ and $x = 1$ for v-component, which is not shown in this paper). In Fig. 9, very large pressure errors exit in the four corners of the computational domain for the Pm II, which is significantly reduced using DPM.

In view of the rate of convergence as well as the temporal errors for the pressure field in cases 1–3, it is apparent that DPM outperforms Pm II significantly. While the pressure convergence rate of Pm II is closely related to the type of boundary conditions, DPM exhibit fully temporally second order behaviors in all the test cases.

5.4. Case 4: lid-driven cavity flows

The 'lid-driven cavity' flows have been established as a standard "benchmark" test for numerical methods of incompressible fluid dynamics. Because the flow field is steady at small Reynolds number, it

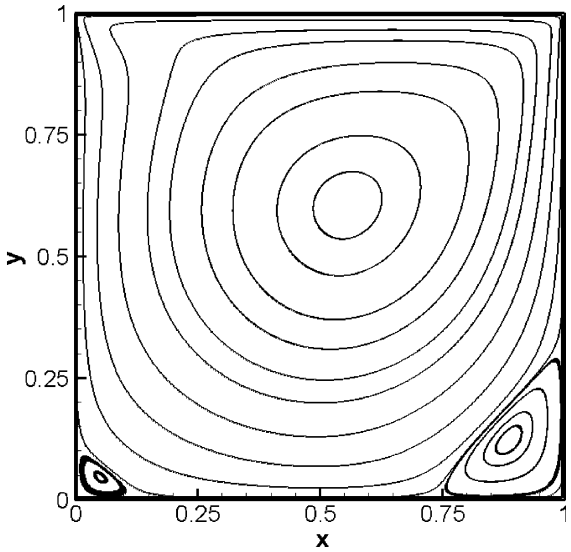

Fig. 10. Streamlines of case 4 when $Re = 400$. Computational results are obtained by DPM with $\Delta t/h = 0.5$ on 128×128 grids.

cannot be used to test the temporal accuracy of the numerical method. However, it is a good case to examine the stability property of the present scheme. Fig. 10 depicts the stream lines of the $Re = 400$ flows in the driven cavity using grids of 128×128. The present method accurately reproduces the formation of the primary and two secondary vortices, with flow structures similar to those given in [12]. Fig. 11 presents a comparison of the velocity distributions at the horizontal centerline of the cavity that are computed using DPM1 and the vorticity-stream-function method [12], respectively. The agreement is excellent. Numerical experiments indicate that DPM1 is stable when $CFL = u\Delta t/\Delta x < 1$.

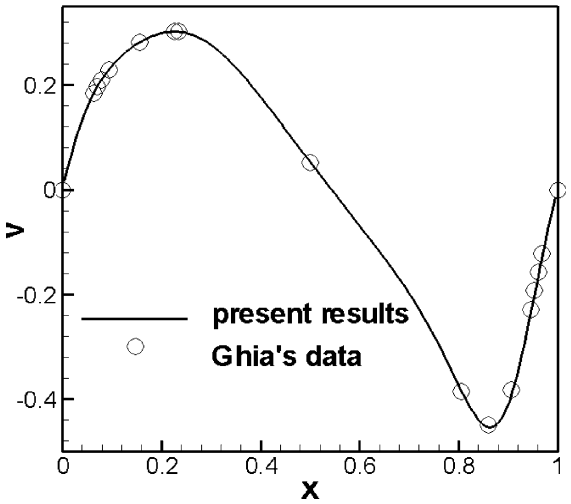

Fig. 11. The v-component velocity profiles at the cavity's horizontal centerline for case 4 when $Re = 400$. Computational results are obtained by DPM and are compared to Ghia's results [12] on 128×128 grids.

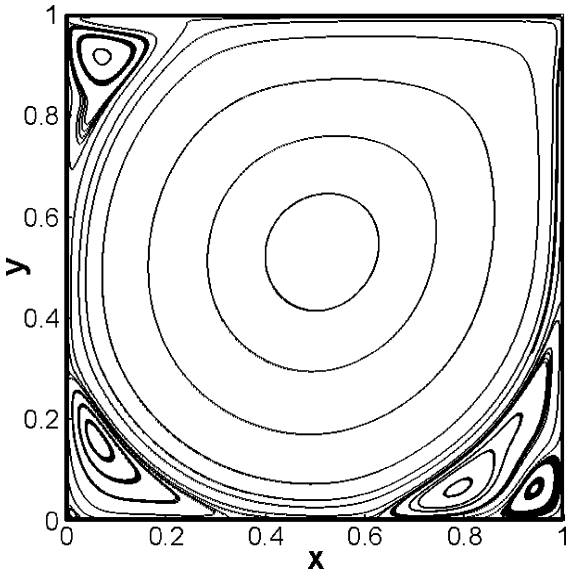

Fig. 12. Streamlines case 4 when $Re = 10{,}000$. Computational results are obtained by DPM with $\Delta t/h = 0.5$ on 128×128 grids.

To examine the performance of the present method for solving the high Reynolds number flows, the $Re = 10{,}000$ flows in the driven cavity have been computed on the 128×128 grids. The numerical result of the stream lines is shown in Fig. 12, the structure of various secondary vortices is in excellent agreement with that reported in [12]. It has been found numerically that DPM1 is stable when $CFL = u\Delta t/\Delta x < 0.75$.

6. Conclusions

In this paper, a continuous projection method is designed and analyzed. The continuous projection method consists of a set of partial differential equations which can be regarded as an approximation of the N–S equations in each interval of a given time discretization. The LTE analysis is employed to analyze continuous projection methods. We find that the rigorous LTE analysis is possible only under artificial boundary conditions in specific forms. This analysis yields a sufficient condition for the continuous projection methods to be temporally second order accurate. Based on this sufficient condition, a class of fully second order accurate continuous projection methods is proposed. The governing equations of the proposed continuous projection method are discretized using second order difference schemes both spatially and temporally, which results in a fully second order accurate discrete projection scheme. A heuristic stability analysis is performed to this projection method showing that the present projection method can be stable. The stability of the present scheme is further verified through numerical tests.

The artificial boundary conditions proposed in this paper ensure the second order accuracy of the velocity and pressure up to the boundary. Therefore, the numerical boundary layer is effectively eliminated. The second order accuracy of the present projection method is confirmed by several numerical test cases.

Acknowledgements

This work was supported by the China NKBRSF (No. 2001CB409600). We thank the referees of this paper for their valuable suggestions to improve the quality of this paper.

References

[1] A.S. Almgren, J.B. Bell, W.G. Szymczak, A numerical method for the incompressible Navier–Stokes equations based on an approximate projection, SIAM J. Sci. Comput. 17 (2) (1996) 358.
[2] J.B. Bell, P. Colella, H.M. Glaz, A second order projection method for the incompressible Navier–Stokes equations, J. Comput. Phys. 85 (1989) 257.
[3] O. Botella, On the solution of the Navier–Stokes equations using Chebyshev projection schemes with third-order accuracy in time, Comput. Fluids 26 (1997) 107.
[4] D.L. Brown, R. Cortez, M.L. Minion, Accurate projection methods for the incompressible Navier–Stokes equations, J. Comput. Phys. 168 (2001) 464.
[5] A.J. Chorin, Numerical solution of the Navier–Stokes equations, Math. Comput. 22 (1968) 745.
[6] A.J. Chorin, On the convergence of discrete approximation to the Navier–Stokes equations, Math. Comput. 23 (1969) 341.
[7] J.K. Dukowicz, A.S. Dvinsky, Approximate factorization as a high order splitting for the implicit incompressible flow equations, J. Comput. Phys. 102 (1992) 336.
[8] W. E, J.-G. Liu, Gauge method for viscous incompressible flows, Commun. Math. Sci. 1 (2) (2003) 317.
[9] W. E, J.-G. Liu, Projection method I: convergence and numerical boundary layers, SIAM J. Numer. Anal. 32 (1995) 1017.
[10] W. E, J.-G. Liu, Projection method II: Godunov–Ryabenki analysis, SIAM J. Numer. Anal. 33 (1996) 1597.
[11] J.H. Ferziger, M. Peric, Computational Methods for Fluid Dynamics, Springer, Berlin, 1996.
[12] U. Ghia, K.N. Ghia, C.T. Shin, High-Re solutions for incompressible flow using the Navier–Stokes equations and a multi-grid method, J. Comput. Phys. 48 (1982) 387.
[13] P.M. Gresho, S.T. Chan, On the theory of semi-implicit projection methods for viscous incompressible flow and its implementation via a finite element method that also introduces a nearly consistent mass matrix. Part 2: implementation, Int. J. Numer. Method Fluids 11 (1990) 621.
[14] P.M. Gresho, On the theory of semi-implicit projection methods for viscous incompressible flow and its implementation via a finite element methods that also introduces a nearly consistent mass matrix. Part 1: theory, Int. J. Numer. Methods Fluids 11 (1990) 587.
[15] P.M. Gresho, R. Sani, On pressure boundary conditions for incompressible Navier–Stokes equations, Int. J. Numer. Methods Fluids 7 (1987) 1111.
[16] J.L. Guermond, J. Shen, A new class of truly consistent splitting schemes for incompressible flows, J. Comput. Phys. 192 (2003) 262.
[17] J.L. Guermond, J. Shen, On the error estimates for the rotational pressure-correction projection methods, Math. Comput. (accepted).
[18] J.L. Guermond, J. Shen, Velocity-correction projection methods for incompressible flows, SIAM J. Numer. Anal. 41 (2003) 112.
[19] M.O. Henriksen, J. Holmen, Algebraic splitting for incompressible Navier–Stokes equations, J. Comput. Phys. 175 (2002) 438.
[20] P. Iannelliand, F.M. Denaro, Analysis of the local truncation error in the pressure-free projection method for incompressible flows, a new accurate expression of the intermediate boundary conditions, Int. J. Numer. Methods Fluids 42 (2003) 309.
[21] G.E. Karniadakis, M. Israeliand, S.A. Orsag, High-order splitting methods for the incompressible Navier–Stokes equations, J. Comput. Phys. 97 (1991) 414.
[22] J. Kim, P. Moin, Application of a fractional-step method to incompressible Navier–Stokes equations, J. Comput. Phys. 59 (1985) 308.
[23] M.L. Minion, D.L. Brown, Performance of under-resolved two-dimensional incompressible flow simulations: II, J. Comput. Phys. 138 (1997) 734.
[24] R.H. Nochetto, J.H. Pyo, Error estimates for semi-discrete Gauge methods for the Navier–Stokes equations: first order schemes. Available from <http://www.math.umd.edu/~rhn/publications.html>.
[25] S.A. Orszag, M. Israeli, M.O. Deville, Boundary conditions for incompressible flows, J. Sci. Comput. 1 (1986) 75.
[26] J.B. Perot, An analysis of the fractional step method, J. Comput. Phys. 108 (1993) 51.
[27] A. Quarteroni, F. Saleri, A. Veneziani, Factorization methods for the numerical approximation of Navier–Stokes equations, Comput. Methods Appl. Mech. Eng . 188 (2000) 505.
[28] J. Shen, On error estimates of the projection methods for the Navier–Stokes equations: first-order schemes, SIAM J. Numer. Anal. 29 (1992) 57.
[29] J. Shen, On error estimates of the projection methods for the Navier–Stokes equations: second-order schemes, Math. Comput. 65 (1996) 1039.
[30] J. Shen, Remarks on the pressure error estimates for the projection methods, Int. J. Numer. Methods Fluids 16 (1993) 249.
[31] J.C. Strikwerda, Y.S. Lee, The accuracy of the fractional step method, SIAM J. Numer. Aanal. 37 (1999) 37.
[32] Y.H. Thomas, B.R. Wetton, Second-order convergence of a projection scheme for the incompressible Navier–Stokes equations with boundaries, SIAM J. Numer. Anal. 30 (3) (1993) 609.

[33] J. van Kan, A second-order accurate pressure-correction scheme for viscous incompressible flow, SIAM J. Sci. Stat. Comput. 7 (3) (1986) 870.
[34] R. vericco, P. Orlandi, A finite-difference scheme for three-dimensional incompressible flows in cylindrical coordinates, J. Comput. Phys. 123 (1996) 402.
[35] C. Wang, J.-G. Liu, Convergence of gauge method for incompressible flow, Math. Comput. 69 (2000) 1385.
[36] B.R. Wetton, Error analysis of pressure increment schemes, SIAM J. Numer. Anal. 38 (2000) 160.